Polymer 81 (2015) 79–86

Contents lists available at ScienceDirect

Polymer

journal homepage: www.elsevier.com/locate/polymer

Polyethylene/reduced graphite oxide nanocomposites with improved morphology and conductivity

Giovani Pavoski [a], Thuany Maraschin [b], Marcéo A. Milani [a], Denise S. Azambuja [a], Raúl Quijada [c], Cássio Stein Moura [d], Nara de Sousa Basso [b], Griselda Barrera Galland [a, *]

[a] Instituto de Química, Universidade Federal do Rio Grande do Sul, Av. Bento Gonçalves, 9500, Porto Alegre 91501-970, Brazil
[b] Faculdade de Química, Pontifícia Universidade Católica do Rio Grande do Sul, Av. Ipiranga 6681, Porto Alegre 90619-900, Brazil
[c] Departamento de Ingeniería Química y Biotecnología, Facultad de Ciencias Físicas y Matemáticas, Universidad de Chile, Casilla, 2777 Santiago, Chile
[d] Faculdade de Física, Pontifícia Universidade Católica do Rio Grande do Sul, Av. Ipiranga, 6681 Porto Alegre, Brazil

ARTICLE INFO

Article history:
Received 4 August 2015
Received in revised form
6 November 2015
Accepted 8 November 2015
Available online 11 November 2015

Keywords:
Polyethylene
Nanocomposites
Graphene
Morphology
Conductivity
Reduced graphite oxide

ABSTRACT

The use of graphite and polyolefins as starting materials to prepare nanocomposites is convenient because both are inexpensive and have very different properties, one is conductive and the other is insulating. The formation of nanocomposites can extend the applicability of both commodities. In this work we synthesized nanocomposites of polyethylene (PE) with two types of graphites, graphite oxide (GO) and reduced graphite oxide (RGO), by *in situ* polymerization using a supported metallocene catalyst. The functional groups on the graphites were used to support the metallocene catalyst by a previous treatment with methylaluminoxane. The nanocomposites were obtained with good catalytic activities and presented excellent morphology and dispersion; their elastic modulus and crystallization temperatures were higher than those of neat PE. However, the nanocomposites PEGO were insulant, whereas PERGO had a conductivity of 1.1×10^{-5} S cm^{-1} with 3.1 wt% filler. This is a significant result compared to the conductivity obtained using non-supported graphite nanosheets where more than 15 wt% of graphite nanosheets are needed to obtain conductivities higher than 10^{-7} S cm^{-1}. This improvement in the percolation threshold was attributed to the good morphology of the PERGO nanocomposites obtained due to the control of the graphitic sheets and the support methodology.

© 2015 Elsevier Ltd. All rights reserved.

1. Introduction

Graphite is found in nature in the form of natural graphite flakes or powders of various particle sizes. Brazil is the third largest producer of graphite, preceded by China and India, and has large reserves [1]. Interest in the graphite industry has dramatically increased with the discovery of the outstanding properties of graphene, the one-atom sheet that composes graphite [2]. However, a major challenge is to obtain adequate quality graphene at an affordable cost. Some current production routes include chemical vapor deposition [3], CO reduction [4], and exfoliating graphite [5–14]. The last method is the only one that can provide large quantities of graphene at a low cost and is the one used to obtain nanocomposites.

Published papers have documented the preparation of polyolefin nanocomposites with graphite or graphite oxide (GO) by blending in the molten state [2,13,15–17], solid-state shear pulverization [18,19] and solution [20,21]. In general, nanoparticles are difficult to disperse. Dispersion of nanoparticles during olefin polymerization benefits from the low viscosity of the liquid polymerization media, which prevents nanoparticle emissions. Dry powder blending with nanoparticles requires special safety precautions and handling procedures to prevent emissions, dust explosions, and health hazards resulting from nanoparticle inhalation or absorption [22]. However, *in situ* polymerization (polymerization of the monomer in the presence of fillers) of ethylene or propylene with graphite or graphite-derivative materials has been less studied [23].

In recent years our research group has been working to obtain graphene/polyolefins nanocomposites using *in situ* polymerization with metallocene catalysts [24–28]. Our results show improvement on the Young modulus, crystallization temperature, thermal stability, and conductivity in the nanocomposites compared with

* Corresponding author.
E-mail address: griselda.barrera@ufrgs.br (G.B. Galland).

http://dx.doi.org/10.1016/j.polymer.2015.11.019
0032-3861/© 2015 Elsevier Ltd. All rights reserved.

neat polymer; however, our electrical percolation threshold was still too high. In that research we used commercially expanded graphite sonicated for 8 h, and we obtained the nanocomposites by *in situ* polymerization using a non-supported approach. However, in some cases, to achieve a homogeneous dispersion of the nanocomposites, covalent functionalization of graphene with polymers may be necessary [29]. There is a growing research focus on introducing covalent linkages between graphene-based filler and the polymer to promote stronger interfacial bonding [30].

Although the functionalization of graphene with polymers is generally attempted with a view to confer new or improved properties to the polymer, the polymer may also prevent the aggregation of the graphene sheets [29–32]. Polypropylene has very recently been grafted from Ziegler–Natta-immobilized GO prepared through a Grignard reagent [33]. Independent of the opposite nature of the polymer and GO, a good dispersion of sheets in the matrix was observed. Strikingly, in spite of the almost insulating nature of GO, good conductivity values were reported. Mülhaupt et al. [22] prepared ultrahigh molecular weight (UHMWPE) graphene nanocomposites supporting a chromium catalyst over functionalized graphene nanosheets recovered by 10% methylaluminoxane (MAO) by the polymerization filling method and obtained good dispersion, mechanical properties, and conductivity. Hu and Liu [34] obtained polyethylene PE/GO nanocomposites using GOs modified with different amines to help in the exfoliation and dispersion of GO in a PE matrix during *in situ* ethylene polymerization with Cp_2ZrCl_2/MAO; however, they did not study the nanocomposite properties.

Based on our experience in the immobilization of metallocene catalysts on different supports [35], in this work we focus on the immobilization of the metallocene catalyst on graphene and the growth of polyolefins from the graphene surface. The objective is to improve graphene exfoliation in the polymeric matrix and consequently improve the nanocomposite properties. We then compared the properties of the nanocomposites already obtained by the non-supported technique with those obtained by the supported approach. There are a number of difficulties in the supporting technique, including the requirement of some functional groups on the graphene to link the catalyst to the graphene surface but at the same time ensuring that those functional groups do not deactivate the catalyst. The immobilization of metallocene catalysts on supports is an alternative approach for utilization of the metallocene catalysts in industrial plants [36]. The ultimate goal in this study is to obtain a conductive material with high processability and good stiffness-to-density ratios so that it can be used in electronic devices for transducers, low-temperature heaters, cellular cells, and also in the aerospace and automotive industries.

2. Experimental

2.1. Materials

All materials were used as received. Graflake 9950 (FK) with a size of around 150 μm was provided by Nacional de Grafite Ltda. (Brazil). Sulfuric acid, nitric acid, hydrochloric acid, and potassium chlorate were purchased from Merck, São Paulo, Brazil.

Polymerization reactions were performed in a 100-ml reactor (Parr Instrument Company, Illinois, USA). The solvents and solutions for polymerization reactions were handled under an inert atmosphere of argon using the standard Schlenk technique. The reagents were used as received, except toluene (Nuclear, Brazil), which was distilled under argon with metallic sodium and benzophenone (Sigma–Aldrich, Brazil) [37].

2.2. Graphite oxide synthesis and thermal reduction

GO was synthesized from FK flakes using a modified Staudenmaier method [38], where the time of oxidation used was 24 h instead of 96 h. The GO was then heated at 1000 °C for 30 s in an oven, using a closed quartz ampoule with normal atmosphere. Reduced graphite oxide (RGO) was obtained.

2.3. Support of the catalyst

For catalyst support, GO or RGO was placed in a Schlenk vessel with toluene using inert atmosphere and was sonicated with a bath (Ultracleaner 1600A, Unique, Brazil) working at 40 kHz for 8 h. The amount of GO and RGO used varied between 100 and 1000 mg. Then, 15% (weight [wt]/wt) MAO was added to the graphite and sonicated for an additional 30 min. Next, Cp_2ZrCl_2 was added in an amount of 2 (wt/wt) Zr/GO or 2% (wt/wt) Zr/RGO, left another 30 min in the ultrasonic bath, and 2 h with stirring at 50 °C. The supernatant was then decanted and the solid washed three times with toluene. Thereafter, the GO/MAO/Cp_2ZrCl_2 or RGO/MAO/Cp_2ZrCl_2 was used as the catalyst for the polymerization of ethylene.

2.4. Polymerization reactions

Polymerization reactions were performed in a 100-ml reactor; toluene was used as the solvent and an additional amount of MAO (Al/Zr = 100) was added as scavenger. The reactions were performed at 70 °C using a 3.0-bar ethylene pressure for 30 min. The polymerization reactions were stopped using ethanol acidified with HCl (10%).

2.5. Characterization

The fractions of C, H, and N in the graphite samples were analyzed using a Perkin–Elmer MCHNSO/2400 analyzer. A sample mass of 2 mg was employed in each analysis.

The contents of zirconium fixed on the nanoparticles were determined by inductively coupled plasma emission spectrometry (ICP) in a Perkin Elmer, Optima 7300.

The melting temperature and crystallinity of the nanocomposites were measured on a differential scanning calorimeter (TA Instruments Q20) with a heating rate of 10 °C min^{-1} and a temperature range of 20–160 °C. The heating cycle was performed twice to remove the thermal history of the material, but only the results of the second heating were considered.

The dynamic mechanical analysis of the nanocomposites was obtained using a DMA analyzer (TA Instrument model Q800). The samples were analyzed in a single cantilevered manner at a frequency of 1 Hz and a strain level of 0.1% in the temperature range of −140 to 120 °C. The heating rate was 3 °C min^{-1}. The tests were conducted using a rectangular bar with dimensions of 17 × 13 × 3 mm.

The analysis of molecular weights was performed on a Waters chromatograph (Alliance GPC 2000) equipped with a differential refractometer and three Styragel HT columns (HT3, HT5, HT6E) previously calibrated with polystyrene standards. The solvent used was 1,2,4-trichlorobenzene at 135 °C. Before injecting the nanocomposites in the chromatograph, samples were placed in a Soxhlet extractor with decalin under reflux for 4 h at 160 °C. The polymers were precipitated from the decalin solution with ethanol, filtered, and dried in a vacuum oven for 4 h.

Scanning Electron Microscopy (SEM) was performed with a Phillips microscope (model XL30) operating at 20 kV, using aluminum stubs and gold metallization.

Transmission Electron Microscopy (TEM) images of the reduced graphene oxide were obtained using a JEOL 2010 TEM operated at 200 kV. All samples were prepared by depositing an acetone suspension drop on a copper grid (300 mesh) covered with amorphous carbon. TEM images of the nanocomposites were obtained using a JEOL 1200 EXII TEM operated at 100 kV. All samples were prepared by depositing an decalin suspension drop on a copper grid (300 mesh) covered with amorphous carbon.

Electrical impedance spectroscopy was performed to measure the electrical conductivity of the graphites. A sine wave with 1.0 Vpp was applied to the sample, and the frequency was varied from 1 to 10^6 Hz. The current and potential differences between the samples' faces were measured. The phase difference between the voltage and current in the sample allows the determination of the real part, which is associated with conductivity, and imaginary parts of electrical impedance. A numerical fitting algorithm was applied to the data, which provided the conductivity values.

Impedance measurements of the nanocomposites were obtained with films cut and sandwiched between two stainless steel electrodes assembled into an epoxy resin holder, as described previously [39]. Film thickness was between 50 and 70 μm, and the area was about 1.5 cm^2. These films were obtained from samples prepared in a Carver Press at 160 °C and 5 ton/cm for 3 min. The measurements were performed using an AUTOLAB PGSTAT 30/FRA 2 in the 1-MHz to 100-mHz frequency range, and the amplitude of the sinusoidal voltage was 10 mV. All experiments were carried out at 25 °C.

3. Results and discussion

Elementary analyses showed that GO consisted of 33% oxygen atoms and that 13% still remained after reduction. Fourier transform infrared (FTIR) spectra (Supplementary data) showed that most of the oxygen is in the form of hydroxyl groups. These functional groups are the ones to which MAO will be fixed, avoiding the deactivation of the metallocene catalyst, which is very sensitive to polar groups. The difference in the number of hydroxyl groups in GO and RGO was also confirm by the amount of catalyst supported.

The quantity of Zr in the supported catalysts was calculated by ICP, and the results were 1.31 wt% Zr/GO and 0.36 wt% Zr/RGO. Considering that initially 2 wt% Zr was placed over the graphite support, the amount of Zr immobilized on the GO showed good results, given that normally only half of the catalyst remains in the support after grafting [35]. This high amount of Zr immobilized over GO can be attributed to the high number of oxygen groups available over GO. On the other hand, the amount of Zr supported over the RGO was only 0.36 wt%, which can be explained by the significantly reduced (2.5 times) number of oxygen groups available in RGO.

Studies of X-ray diffraction (XRD) (Supplementary data), Raman (Supplementary data), SEM and TEM (Fig. 1 and Supplementary data) of these graphites showed that they are constituted by graphene sheets (an average of 11 graphenes per crystal) with a distance between the graphenes of 0.8 nm in GO and 0.35 nm in RGO. As one of the objectives of this work was to compare the nanocomposites obtained by the supported method (this work) with the results obtained in our previous work, we included some of the published results. We previously used the non-supported method [23,25–28], i.e., we placed the graphite, MAO, catalyst, and monomer together in the reactor without supporting the catalyst first. In order to avoid the deactivation of the catalyst, the graphite used was sonicated expanded graphite (GNS) with a very low percentage of oxygen (2.4%), as described previously [24].

Table 1 shows the results of the polymerization of ethylene with the catalysts supported on GO and RGO. The results of the homogeneous polymerization of ethylene and the results obtained with GNS using the *in situ* polymerization (non-supported method) are also shown. In the case of the supported catalyst systems, the ratio of Al/Zr used in the reactor was 100 because the supported catalysts already have MAO impregnated in the support. In this case, the amount of MAO in the reactor works only as a scavenger because the catalyst was already activated by the MAO in the support. For the *in situ* polymerizations with GNS, the Al/Zr used was 1000 because MAO needs to act as a scavenger and an activator.

In the polymerizations with the system Cp_2ZrCl_2/MAO/GO, there was a decrease in the catalytic activity with an increase in the amount of graphite in the support, probably due to the high number of oxygen groups even though the amount of MAO was also increased. In all cases these catalytic activities were inferior to the ones obtained with the reduced oxide that contained fewer deactivating functional groups. The catalytic activities of the supported catalysts were lower than the ones presented by the homogeneous *in situ* polymerization. This behavior is normally observed in heterogeneous systems because not all the Zr impregnated in the support are actives, as is the case in homogeneous polymerization [35].

Melting temperatures (Tm) and crystallinities (Xc) of the nanocomposites did not show a trend; however, the crystallization temperatures (Tc) of all the nanocomposites were 2–4 °C higher than those of the neat PE, showing the nucleation power of the filler. Mass average molecular weights of the supported nanocomposites (PEGO: molecular weight (M_W) = 50,000 g mol^{-1} and the polydispersities between 2.0 and 2.8), were all significantly higher than the ones obtained with homogeneous polymerization (PE: M_W = 28,000 g mol^{-1} and polydispersity of 3.0), which is typical of the heterogeneous catalyst [35].

The nanocomposite morphology was studied by SEM. Fig. 1 shows the SEM images of all the graphites compared in this work; GO, RGO, and GNS, were all highly exfoliated. TEM of RGO and GNS are also shown in Fig. 1. It is possible to count the number of graphenes in the nanosheets (see the sheet between the arrows in Fig. 1d), confirming that RGO is composed by a few graphene layers as it was also estimated by XRD (Supporting information). In GNS the number of graphenes per sheet was higher.

Figs. 2 and 3 show different SEM magnifications of the PEGO2 and PERGO1 nanocomposites with similar amounts of filler (2.5 and 2.2 wt%, respectively). For comparison, Fig. 4 shows the SEM of PE obtained by homogeneous polymerization (Fig. 4a) and two SEM magnifications (b) and (c) of the nanocomposite PEGNS2 (with 2.8 wt% of GNS) obtained by *in situ* polymerization; the differences in morphology are impressive. The nanocomposites obtained with the supported catalysts (Figs. 2 and 3) formed spherical particles that flowed easily, preventing the fouling of the reactor. The non-supported catalyst gave nanocomposites with morphology closer to PE (Fig. 4). The nanocomposite obtained with the RGO had a highly exfoliated structure (Fig. 3d), showing that PE grew over the exfoliated graphite sheets. The PEGO nanocomposites were also very exfoliated, but the blades of graphite were not as ordered as in the PERGO (Figs. 2d and 3d).

Transmission electronic micrographs of the nanocomposites with GO and RGO are shown in Fig. 5. It can be seen like dark worms (Fig. 5a and c) distributed uniformly all over the samples that represent graphite nanosheets with very good aspect ratio recovered by polymer. In the higher magnification micrographs (Fig. 5b and d) it can be seen dark lines in the thinner part of the sample showing the graphene nanosheets. In both samples the filler seems to have a very good dispersion in the polymeric matrix.

Dynamic mechanical studies (Fig. 6) showed that the storage modulus (E′) is higher in all the nanocomposites compared to the neat polymer, showing a significant increase in stiffness and

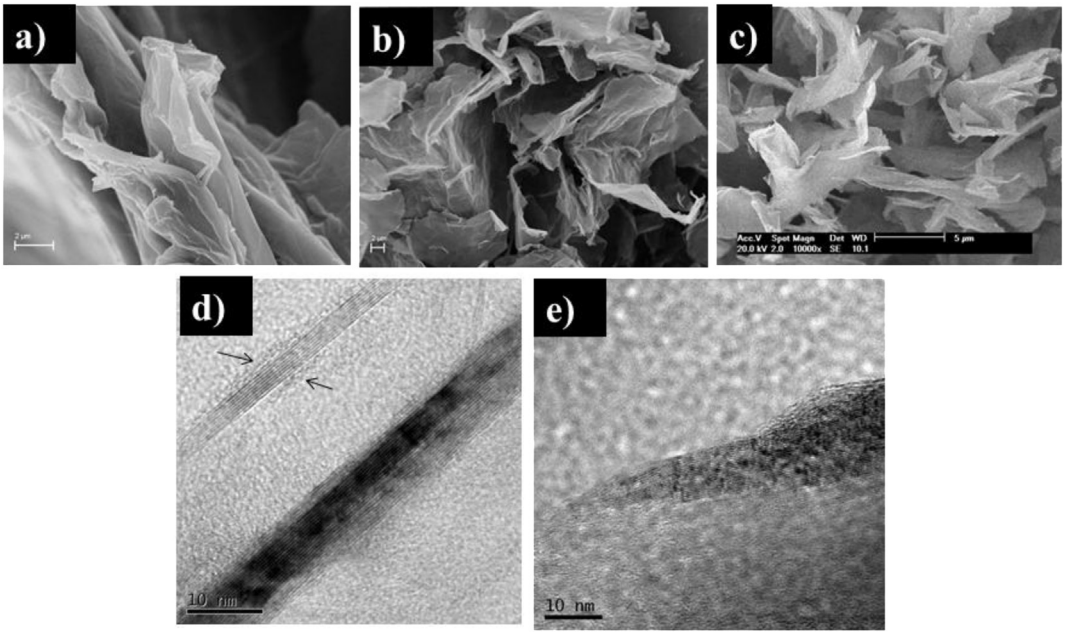

Fig. 1. SEM of (a) GO, (b) RGO and (c) GNS and TEM of (d) RGO and (e) GNS [24].

Table 1
Nanocomposites of polyethylene with different graphites, catalytic activities, and thermal properties.

Samples	Graphites (%)	Graphites (g)	Polymer (g)	Catalytic activity (KgPE/[Zr] h bar)	T_c (°C)	T_m (°C)	X_c (%)	T_g (°C)
PE	0	0	10.9	166	116	131	69	−113.2
PEGO1	1.1	0.1	8.9	415	118	132	78	−111.1
PEGO2	2.5	0.2	7.9	182	117	133	84	−111.6
PEGO3	3.0	0.3	9.9	153	118	132	90	–
PEGO4	9.5	0.5	5.3	49	119	134	78	−111.2
PERGO1	2.2	0.2	9.2	780	119	134	–	−111.5
PERGO2	3.1	0.3	9.6	544	120	132	66	–
PEGNS1[a]	1.2	0.05	4.1	1464	118	132	72	−109
PEGNS2[a]	2.8	0.1	3.6	1285	118	131	73	−109
PEGNS3[a]	5.6	0.2	4.6	1642	119	132	84	−106

PEGO = nanocomposite of polyethylene with graphite oxide; PERGO = nanocomposite of polyethylene with reduced graphite oxide; PEGNS: nanocomposite of polyethylene with graphite nanosheets.
[a] Samples prepared by *in situ* polymerization with Graphene Nanosheets (GNS) using the non-supported method. This data is described in Refs. [24,27].

reinforcement. Graphite fillers make the polymer stiffer when they are well dispersed [40]. Once that the DMA analysis takes into account the viscoelastic behavior of the polymer, the modulus measured in this analysis is not exactly the same to the Young's modulus of the classic stress–strain curve. However, as the storage modulus is associated with a rigid material, it may be related to the Young's modulus especially in the room temperature region [41,42]. At 25 °C nanocomposites with similar amount of filler, PEGO2 (2.5%) and PERGO1 (2.2%) show the same E′ of 2100 MPa. This value is 75% superior to the one presented by the neat polyethylene (1200 MPa). When the GO content added was 9.5% (PEGO4) the value found for E' (2300 MPa) was almost doubled. Such important enhancement in the storage and/or Young modulus have been seen in other studies when graphite-based fillers were considered well dispersed in the matrix [18,22,26,27].

These data as well as the transition temperature (Table 1), which was higher in the nanocomposites, showed the reinforcement effect of the fillers, which depends more on the amount than on the type of graphite.

One of the aims of this study is to transform an insulant material as PE to a semi-conductor material to broaden the applications. Table 2 shows the conductivities of the fillers (GO, RGO and GNS) and their PE nanocomposites. The presence of almost 33% oxygen atoms in GO should make this graphite the least conductive among the studied ones, and this was the case in our study. However, 1.2×10^{-2} S cm^{-1} is also good average conductivity given that the measurement of conductivity is made of a pellet without any orientation. Graphite is an anisotropic material that presents conductivity only in one direction, i.e., in the horizontal plane, so this method obtained an average conductivity. GNS, which has only 2.4% oxygen, is only two times more conductive than GO; on the other hand, RGO with about 13% oxygen is 10 times more conductive than GO. The presence of oxygen, therefore, is not the only factor influencing conductivity. Previous studies [24] (see also Supplementary data) shows that RGO is more exfoliated than GNS and has fewer graphenes per sheet. This difference in the type of graphite used has an appreciable influence on the conductivity of the nanocomposites produced. In the case of the nanocomposites obtained with GO, neither of them were conductive even using a high amount of filler (9.5%). The nanocomposites obtained with GNS using the *in situ* polymerization [27], i.e., mixing all the reagents in the reactor without previous support of the catalyst, gave conductive nanocomposites but only when a high amount of graphite was used—15.3 wt% and 20.9 wt% GNS to obtain

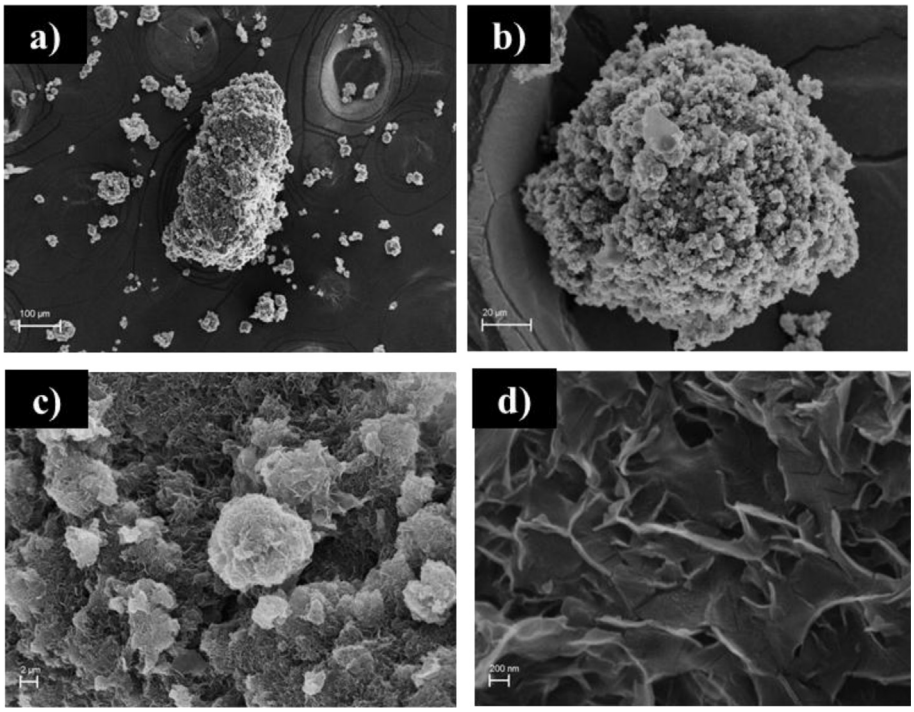

Fig. 2. SEM images of nanocomposite PEGO2 (2.5% GO/PE) at different magnifications, scale bars: a) 100 μm, b) 20 μm, c) 2 μm and d) 200 nm.

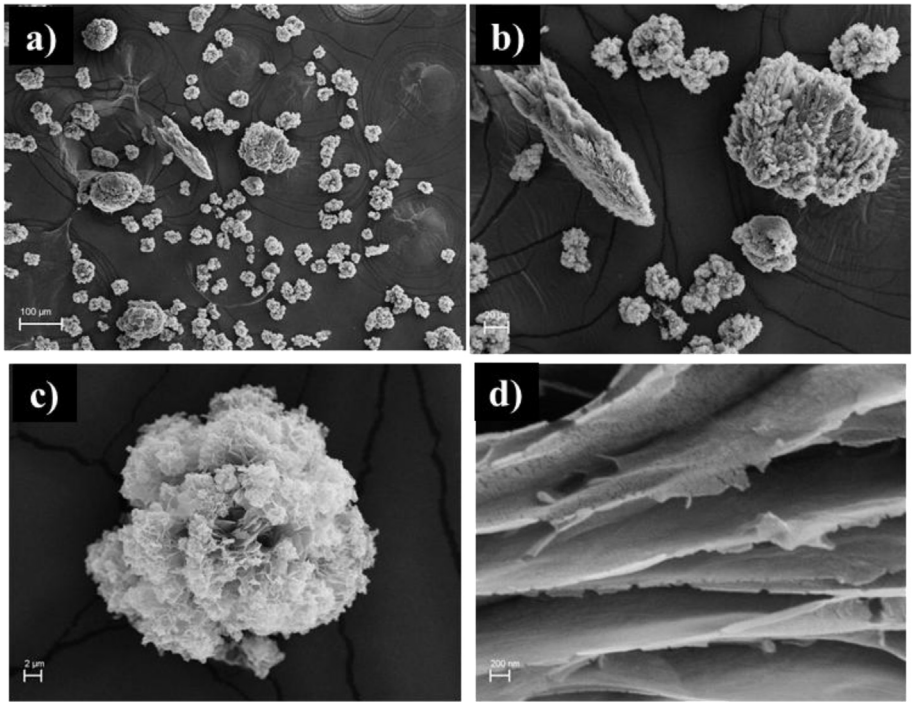

Fig. 3. SEM images of nanocomposites PERGO1 (2.2% RGO/PE) at different magnifications, scale bars: a) 100 μm, b) 20 μm, c) 2 μm and d) 200 nm.

conductivities of 1.6×10^{-7} and 1.3×10^{-4} S cm^{-1}, respectively. Remarkably, RGO gave an PERGO nanocomposite having a conductivity of 1.1×10^{-5} S cm^{-1}with only 3.1 wt% of RGO distributed in the PE matrix.

This strong decrease in the percolation threshold can be attributed to two factors. The first is the excellent exfoliation of this RGO, the quality of the graphene sheets with a low number of defects, and possibly the presence of single graphene sheets that provided a better dispersion in the matrix. The second factor is the methodology used, which was supporting the catalyst that led to the morphology of the graphene sheets. It can be seen in Fig. 3 that the PE-recovered graphene sheets are almost parallel or orientated, which significantly enhance conductivity. On the other hand, Fig. 2 shows that the nanocomposite sheets in PEGO are disordered,

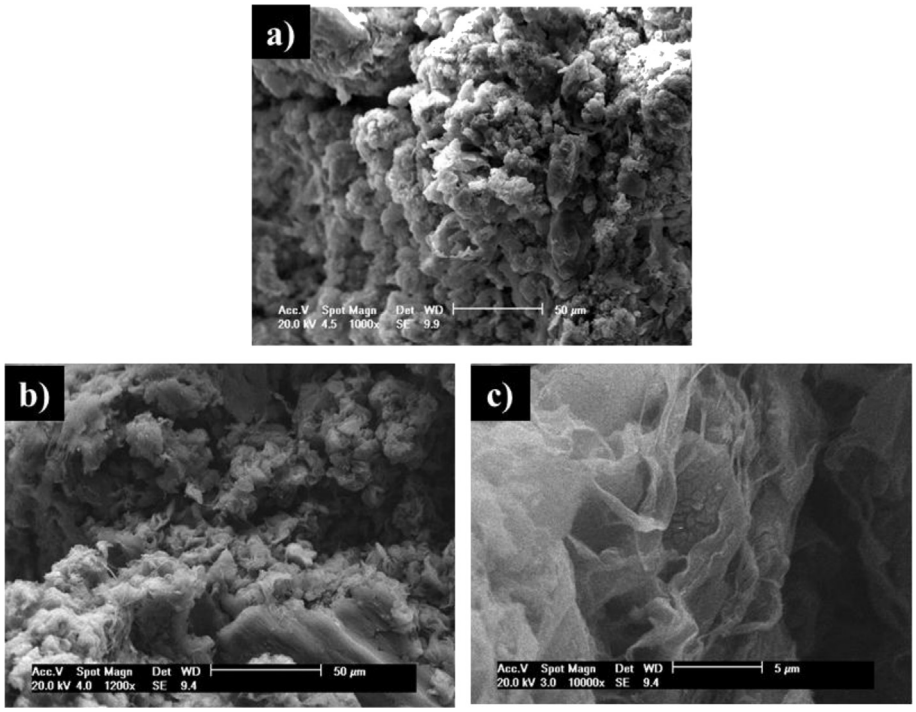

Fig. 4. SEM images of a) PE, scale bar 50 μm and PEGNS 2.8% *in situ* polymerization, scale bars: b) 50 μm and c) 5 μm.

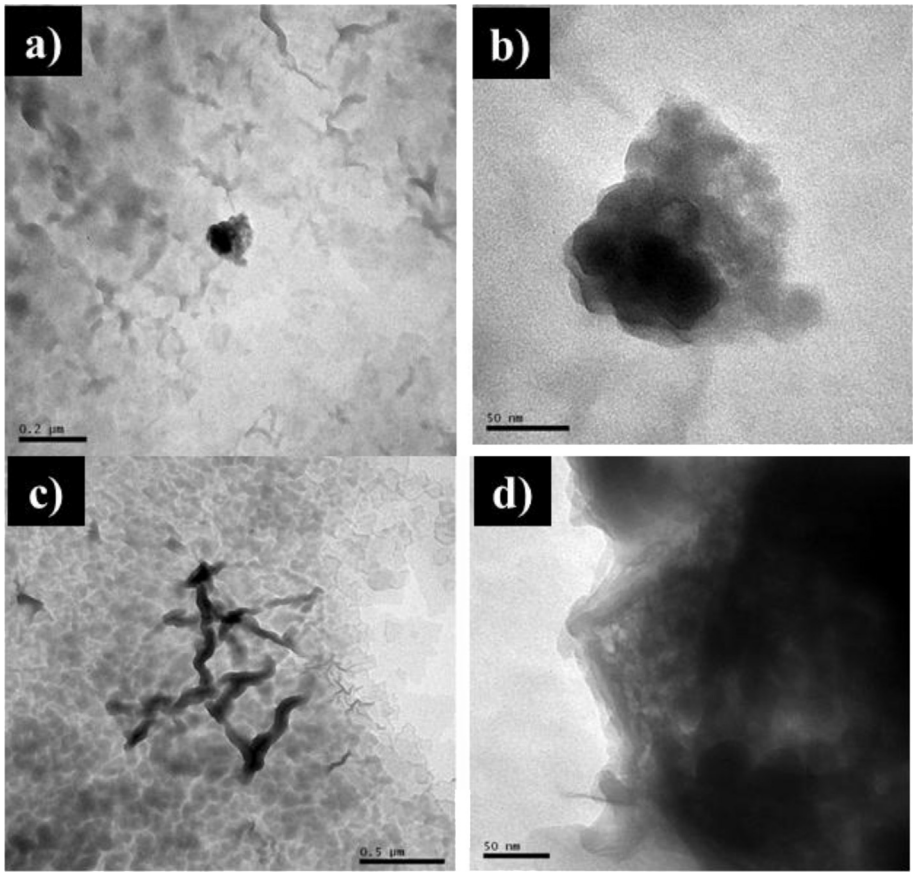

Fig. 5. TEM image of PEGO2 (2.5%) with scale bars a) 0.2 μm and b) 50 nm and PERGO1 (2.2%), scale bars c) 0.5 μm and d) 50 nm.

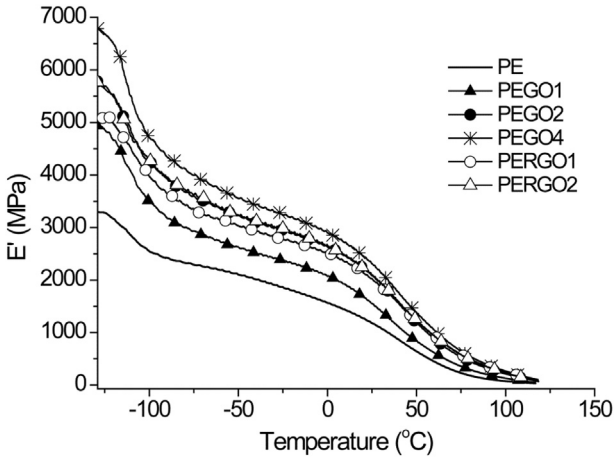

Fig. 6. Variation of the Storage modulus (E′) with temperature of the nanocomposites of PEGO and PERGO.

Table 2
Conductivities of the samples obtained by electrical impedance spectroscopy.

Sample	Graphite (wt.%)	Conductivity (S cm^{-1})
GO	100	1.2×10^{-2}
RGO	100	1.7×10^{-1}
GNS	100	3.5×10^{-2}
PE	0	1.4×10^{-13}
PEGO4	9.5	1.5×10^{-12}
PERGO1	2.2	8.5×10^{-8}
PERGO2	3.1	1.1×10^{-5}
PEGNS2[a]	2.8	1.5×10^{-12}
PEGNS4[a]	15.3	1.6×10^{-7}
PEGNS5[a]	20.9	1.3×10^{-4}

[a] Data from Ref. [27].

which does not provide good conductivity. To our knowledge, this is the first work where these types of morphologies are shown.

4. Conclusions

PERGO nanocomposites with excellent morphology and good conductivity were obtained. The key to obtaining this interesting material is the preparation of a high exfoliated graphite with a low number of defects and some oxygen functional groups (13%) on the surface as support in the *in situ* polymerization of ethylene. The nanocomposite was obtained in the form of spherical particles that flowed easily. A closer view of these particles shows that they are formed by parallel sheets of graphene recovered by polyethylene. This morphology and the good dispersion of the filler in the matrix resulted in an improved conductivity compared with that of the nanocomposites obtained by the *in situ* polymerization with the non-supported approach.

Acknowledgments

The authors would like to thank CNPq 302902/2013-9 and 473128/2011-0, CAPES, FAPERG-PRONEX 09/2009, Department of the Navy Grant N62909-11-1-7069 issued by Office of Naval Research Global, PROYECTO FONDECYT: 1130446 for financial support. R.Q. acknowledge the Millennium Nucleus of Chemical Processes and Catalysis (CPC), grant number NC120082. We also thank Nacional de Grafite Ltda./Brazil for the Graflake 9950 supply and CME and LRNANO from UFRGS for microscopy analysis.

Appendix A. Supplementary data

Supplementary data related to this article can be found at http://dx.doi.org/10.1016/j.polymer.2015.11.019.

References

[1] http://www.mme.gov.br/portalmme/opencms/sgm/galerias/arquivos/plano_duo_decenal/a_mineracao_brasileira/P28_RT41_Perfil_da_Grafita.pdf.
[2] T.G. Gopakumar, D.J.Y.S. Pagé, Polypropylene/graphite nanocomposites by thermo-kinetic mixing, Polym. Eng. Sci. 44 (2004) 1162–1169.
[3] (a) S.J. Chae, F. Günes, K.K. Kim, E.S. Kim, G.H. Han, S.M. Kim, H.-J. Shin, S.-M. Yoon, J.-Y. Choi, M.H. Park, C.W. Yang, D. Pribat, Y.H. Lee, Synthesis of large-area graphene layers on nickel film by chemical vapor deposition: wrinkle formation, Adv. Mater. 21 (2009) 2328–2333;
(b) C. Di, D. Wei, G. Yu, Y. Liu, Y. Guo, D. Zhu, Patterned graphene as source/drain electrodes for bottom-contact organic field-effect transistors, Adv. Mater. 20 (2008) 3289–3293.
[4] C.D. Kim, B.K. Min, W.S. Jung, Preparation of graphene sheets by the reduction of carbon monoxide, Carbon 47 (2009) 1610–1612.
[5] K.S. Novoselov, A.K. Geim, S.V. Morozov, D. Jiang, Y. Zhang, S.V. Dubonos, et al., Electric field effect in atomically thin carbon films, Science 306 (5696) (2004) 666–669.
[6] G. Chen, C. Wu, W. Weng, D. Wu, W. Yan, Preparation of polystyrene/graphite nanosheet composite, Polymer 44 (2003) 1781–1784.
[7] B. Debelak, K. Lafdi, Use of exfoliated graphite filler to enhance polymer physical properties, Carbon 45 (2007) 1727–1734.
[8] V. Yakovlev, A.I. Finaenov, S.L. Zabud'kov, E.V. Yakovleva, Thermally expanded. graphite: synthesis, properties, and prospect for use, Russ. J. Appl. Chem. 79 (2006) 1741–1751.
[9] J. Li, Q. Liu, H. Da, Preparation of sulfur-free exfoliated graphite at a low exfoliation temperature, Mater. Lett. 61 (2007) 1832–1834.
[10] G.H. Chen, D.J. Wu, W.G. Weng, W.L. Yan, Preparation of polymer/graphite conducting nanocomposite by intercalation polymerization, J. Appl. Polym. Sci. 82 (2001) 2506–2513.
[11] G.H. Chen, D.J. Wu, W.G. Weng, W.L. Yan, Dispersion of graphite nanosheets in a polymer matrix and the conducting property of the nanocomposites, Polym. Eng. Sci. 41 (2001) 2148–2154.
[12] X.S. Du, M. Xiao, Y.Z. Meng, Facile synthesis of highly conductive polyaniline/graphite nanocomposites, Eur. Polym. J. 40 (2004) 1489–1493.
[13] K. Kalaitzidou, H. Fukushima, L.T. Drzal, Mechanical properties and morphological characterization of exfoliated graphite–polypropylene nanocompósitos, Compos. Part A 38 (2007) 1675–1682.
[14] L.M. Viculis, J.J. Mack, O.M. Mayer, H.T. Hahnb, R.B. Kaner, Intercalation and exfoliation routes to graphite nanoplatelets, J. Mater. Chem. 15 (2005) 974–978.
[15] K. Kalaitzidou, H. Fukushima, L.T. Drzal, Multifunctional polypropylene composites produced by incorporation of exfoliated graphite nanoplatelets, Carbon 45 (2007) 1446–1452.
[16] K. Kalaitzidou, H. Fukushima, H. Miyagawa, L.T. Drzal, Flexural and tensile moduli of polypropylene nanocomposites and comparison of experimental data to Halpin-Tsai and Tandon-Weng models, Polym. Eng. Sci. 47 (2007) 1796–1803.
[17] P. Steurer, R. Wissert, R. Thomann, R. Mülhaupt, Functionalized graphenes and thermoplastic nanocomposites based upon expanded graphite oxide, Macromol. Rapid Commun. 30 (2009) 316–327.
[18] K. Wakabayashi, C. Pierre, D.A. Dikin, R.S. Ruoff, T. Ramanathan, L.C. Brinson, J.M. Torkelson, Polymer–graphite nanocomposites: effective dispersion and major property enhancement via solid-state shear pulverization, Macromolecules 41 (2008) 1905–1908.
[19] K. Wakabayashi, P.J. Brunner, J. Masuda, S.A. Hewlett, J.M. Torkelson, Polypropylene-graphite nanocomposites made by solid-state shear pulverization: Effects of significantly exfoliated, unmodified graphite content on physical, mechanical and electrical properties, Polymer 51 (2010) 5525–5531.
[20] P. Song, Z. Cao, Y. Cai, L. Zhao, Z. Fang, S. Fu, Fabrication of exfoliated graphene-based polypropylene nanocomposites with enhanced mechanical and thermal properties, Polymer 52 (2011) 4001–4010.
[21] V. Panwar, J.O. Park, S.H. Park, S. Kumar, R.M. Mehra, Electrical, dielectric, and electromagnetic shielding properties of polypropylene-graphite composites, J. Appl. Polym. Sci. 115 (2010) 1306–1314.
[22] M. Stürzel, F. Kempe, T. Yi, S. Mark, M. Enders, R. Mülhaupt, Novel graphene UHMWPE nanocomposites prepared by polymerization filling using single-site catalysts supported on functionalized graphene nanosheet dispersions, Macromolecules 45 (2012) 6878–6887.
[23] J.R. Potts, D.R. Dreyer, C.W. Bielawski, R.S. Ruoff, Graphene-based polymer nanocomposites, Polymer 52 (2011) 5–25.
[24] F.C. Fim, J.M. Guterres, N.R.S. Basso, G.B. Galland, Polyethylene/graphite nanocomposites obtained by *in situ* polymerization, J. Polym. Sci. Part A Polym. Chem. 48 (2010) 692–698.
[25] M.A. Milani, R. Quijada, N.R.S. Basso, A.P. Graebin, G.B. Galland, Influence of the graphite type on the synthesis of polypropylene/graphene nanocomposites, J. Polym. Sci. Part A Polym. Chem. 50 (2012) 3598–3605.
[26] M.A. Milani, D. González, R. Quijada, N.R.S. Basso, M.L. Cerrada, D.S. Azambuja,

G.B. Galland, Polypropylene/graphene nanosheet nanocomposites by *in situ* polymerization: synthesis, characterization and fundamental properties, Compos. Sci. Technol. 84 (2013) 1–7.
[27] F.C. Fim, N.R.S. Basso, A.P. Graebin, D.S. Azambuja, G.B. Galland, Thermal, electrical, and mechanical properties of polyethylene–graphene nanocomposites obtained by *in situ* polymerization, J. Appl. Polym. Sci. 128 (2013) 2630–2637.
[28] M.A. Milani, D. González, R. Quijada, R. Benavente, J. Arranz-Andrés, G.B. Galland, Synthesis, characterization and properties of poly(propylene-1-octene)/graphite nanosheet nanocomposites obtained by *in situ* polymerization, Polymer 65 (2015) 134–142.
[29] M. Zhang, Y. Li, Z. Su, G. Wei, Recent advances in the synthesis and applications of graphene-polymer nanocomposites, Polym. Chem. 6 (2015) 6107–6124.
[30] H.J. Salavagione, G. Martinez, G. Ellis, Recent advances in the covalent modification of graphene with polymers, Macromol. Rapid Commun. 32 (2011) 1771–1789.
[31] L. Meli, A. Arceo, P.F. Green, Control of the entropic interactions and phase behavior of a thermal nanoparticle/homopolymer thin film mixtures, Soft Matter 5 (2009) 533–537.
[32] M.A. Yaklin, P.M. Duxbury, M.E. Mackay, Control of nanoparticle dispersion in thin polymer films, Soft Matter 4 (2008) 2441–2447.
[33] Y. Huang, Y. Qin, Y. Zhou, H. Niu, Z.Z. Yu, J.Y. Dong, Polypropylene/graphene oxide nanocomposites prepared by in situ Ziegler-Natta polymerization, Chem. Mater. 22 (2010) 4096–4102.
[34] Z. Hu, C. Liu, Polyethylene/graphite oxide nanocomposites obtained by in situ polymerization using modified graphite oxide–supported metallocene catalysts, J. Polym. Res. 20 (2013) 39–46.
[35] a) G.B. Galland, M. Seferin, R.S. Mauler, J.H.Z. dos Santos, Linear low-density polyethylene synthesis promoted by homogeneous and supported catalysts, Polym. Int. 48 (1999) 660–664;
b) G.B. Galland, J.H.Z. dos Santos, F.C. Stedile, P.P. Greco, A.D. Campani, Evaluation of silica-supported zirconocenes in ethylene/1-hexene copolymerization, J. Mol. Catal. Part A Chem. 210 (2004) 149–156;
c) T. Velilla, K. Delgado, R. Quijada, D. Bianchini, G.B. Galland, J.H.Z. dos Santos, D.P. Fasce, R.J.J. Williams, New architecture of supported metallocene catalysts for alkene polymerization, J. Polym. Sci. Part A Polym. Chem. 45 (2007) 5480–5486;
d) D. Bianchini, G.B. Galland, J.H.Z. dos Santos, D.P. Fasce, I.E. Dell'Erba, R. Quijada, M. Perez, Metallocene supported on a polyhedral oligomeric silsesquioxane-modified silica with high catalytic activity for ethylene polymerization, J. Polym. Sci. Part A Polym. Chem. 43 (2005) 5465–5476.
[36] G.G. Hlatky, in: J. Scheirs, W. Kaminsky (Eds.), Metallocene-based Polyolefins, vol. 1, Wiley, West Sussex, UK, 2000, pp. 201–218.
[37] W. Amarego, D. Perrin, in: 4º ed.Purification of Laboratory Chemicals, 1997.
[38] L. Staudenmaier, Verfahren zur darstellung der graphitsaure, Ber. Dtsch. Chem. Ges. 31 (1898) 1481–1487.
[39] I.R. Rodrigues, M.M.C. Forte, D.S. Azambuja, K.R.L. Castagno, Synthesis and characterization of hybrid polymeric networks (HPN) based on polyvinyl alcohol/chitosan, React. Funct. Polym. 67 (2007) 708–715.
[40] A.D. Todd, C.W. Bielawski, Thermally reduced graphite oxide reinforced polyethylene composites: a mild synthetic approach, Polymer 54 (2013) 4427–4430.
[41] K.P. Menard, Dynamic Mechanical Analysis, CRC Press, Boca Raton, US, 2008.
[42] H. Zhou, Investigation of Toner Adhesion in the Electrophotographic Process, Cuvillier Verlag, Göttingen, GER, 2008.